First-principles study of migration, restructuring, and dissociation energies of oxygen complexes in silicon

Young Joo Lee, J. von Boehm, M. Pesola, and R. M. Nieminen

COMP/Laboratory of Physics, Helsinki University of Technology, P.O. Box 1100, FIN-02015 HUT, Finland

Migration, restructuring, and dissociation energies of oxygen complexes in silicon are studied theoretically through density-functional total-energy calculations. We find that the stablest oxygen complexes are straight chains that also have the lowest migration energies. The calculated migration energies decrease from 2.3 eV for an interstitial oxygen atom (O_i) to low values of 0.4–1.6 eV for O_2–O_9 chains and 1.9–2.2 eV for longer chains. The oxygen chains (which are thermal double donors) are expected to grow so that the migrating oxygen chains capture less-mobile but abundant O_i's: $O_n + O_i \rightarrow O_{n+1}$. Restructuring energies of chains with a side O_i into straight oxygen chains are 1.9–2.5 eV. Restructuring gives an essential contribution to the fast diffusion. We find that the shorter O_2–O_9 chains dissociate primarily by ejecting one of the outermost oxygen atoms.

I. INTRODUCTION

Czochralski-grown silicon has a high concentration of oxygen (typically 10^{18} O atoms/cm^3).[1] Individual oxygen atoms occupy interstitial bond-center positions.[2] The interstitial oxygen atoms (O_i) diffuse by hopping between neighboring bond-center sites with an activation energy of 2.5 eV in a wide range of temperatures 300–1200 °C.[2,3] Clustering of oxygen occurring under the heat treatments during manufacturing processes is a natural consequence due to the supersaturation of oxygen. Quartz precipitates have been observed at high temperatures (> 800 °C).[4] The formation process of precipitates is found to be governed by the diffusion of O_i. At lower temperatures, especially in the range of 350–500 °C, oxygen clustering gives rise to different types of aggregates—the so-called thermal donors. The thermal donors appear as three families: the thermal double donors (TDD's), shallow thermal donors, and new thermal donors.[5–9] The presence of thermal donors significantly degrades the performance of the Si wafers used for integrated circuits, and TDD's are probably among the most studied defects in semiconductors. It is commonly believed that TDD's have a common core to which oxygen atoms aggregate to form a series of closely related TDD's.[1] The mechanism and kinetics of the TDD formation are not well understood.[1,10–12] The main reason is that the kinetics of the TDD formation cannot be explained with the normal O_i diffusivity because it is too low (the activation energy of 2.5 eV is too high) to explain the observed fast TDD formation occuring with a low activation energy of 1.7 eV.[13–16]

Several models have been suggested when trying to relate the clustering of oxygen to the formation kinetics of TDD's. Almost all models assume an oxygen-containing fast-diffusing species (FDS) with a low activation energy for migration.[17,18] The model based on oxygen clustering seems to be most attractive because it can consistently explain the second-order process of O_i loss[17,19] monitored by infrared-absorption experiments.[18–20]

A popular model used to describe the TDD formation as-sumes that only the oxygen dimer (O_2) acts as a FDS.[20,21] The TDD formation would then proceed as follows:[11,17,20,22,23]

$$O_2 + O_2 \rightleftharpoons TDD1,$$

$$O_2 + TDD1 \rightleftharpoons TDD2,$$

$$O_2 + TDD2 \rightleftharpoons TDD3,$$

$$\vdots . \tag{1}$$
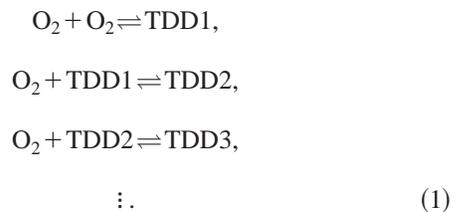
In this model, the TDD's are immobile. However, extremely high values of O_2 diffusivity are required to account for the successive reactions in Eq. (1).[22] In the second model, proposed by Murin and Markevich,[22] first TDD's act as FDS and the formation of TDD's proceeds as follows:

$$O_2 + O_i \rightleftharpoons O_3,$$

$$O_3 + O_i \rightleftharpoons TDD0,$$

$$TDD0 + O_i \rightleftharpoons TDD1,$$

$$TDD1 + O_i \rightleftharpoons TDD2,$$

$$\vdots . \tag{2}$$
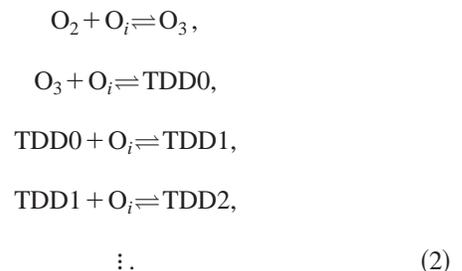
The basic ingredients in kinetic models are the activation energies for migration (or migration energies in short) as well as the restructuring, formation, and binding energies for various oxygen clusters influencing directly what kind of kinetics the TDD formation follows. Earlier calculations have shown that the migration energy of O_2 is roughly half that of O_i.[24–29] The purpose of this paper is to report calculated energies for a large number of oxygen complexes obtained from accurate total-energy calculations and to study qualitatively the kinetics of the TDD formation on the basis of these energies. The energies are used in a general kinetic model that will be reported in a forthcoming publication.[30] A short report of this work has appeared earlier.[24]

The format of this paper is as follows. The computational methods are presented in Sec. II. The migration of oxygen complexes is considered in Sec. III, and the energies and their implications for cluster reactions are presented in Sec. IV. The conclusions are drawn in Sec. V.

II. COMPUTATIONAL METHODS

The total-energy calculations are performed using the density-functional theory[31] in the local-density approximation.[32] The calculations are performed using a self-consistent total-energy pseudopotential (PP) method.[33,34] The Perdew-Zunger parametrization[35] of the Ceperley-Alder data[36] is used for the exchange-correlation energy. For silicon the norm-conserving Hamann[37] PP including the nonlinear core-valence exchange-correlation corrections is used. The Hamann PP is of the fully separable Kleinman-Bylander form[38] and the s component is used as the local one. The ultrasoft Vanderbilt[39] PP is used for oxygen. A well-converged plane-wave basis set with a cutoff energy of 28 Ry is used for the valence-electron wave functions. The Γ-point sampling and cubic 128 atom-site supercells or elongated 108 and 162 atom-site supercells are used. The elongated supercells allow us to study long oxygen chains, because the intersupercell $[1\bar{1}0]$ distances are in this case about 22 and 35 Å for the 108 and 162 atom-site supercell, respectively. The supercell size, the lattice constant, and the cutoff energy were tested in previous calculations.[40–43]

The structures are obtained by allowing all ionic coordinates to relax without any constraints until the largest remaining Hellman-Feynman force component is less than 1 meV/Å. The migration paths and barriers are obtained by moving the oxygen complexes as follows. A chosen (but otherwise arbitrary) O or Si atom of the oxygen complex considered is bound to move in the plane perpendicular to the jump-defining vector connecting its initial and final positions.[44,45] All other atoms are allowed to relax without constraints. The plane is moved in steps of 0.02–0.1 Å. The migration energies are calculated from the formation energy:
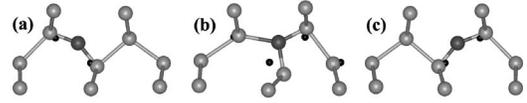
FIG. 1. The diffusive jump of an oxygen atom (black ball) between neighboring bond centers. Grey balls represent silicon atoms. Black dots denote the equilibrium positions of the silicon atoms. (a) Initial O_i position. (b) Saddle-point configuration. (c) Final O_i position.

$$E_f(Q,\mu_e) = E_d(Q) + Q \cdot (E_v + \mu_e) - \sum_s n_s \mu_s, \quad (3)$$

where Q is the charge of the supercell in units of elementary charge, $E_d(Q)$ is the total energy in the charge state Q, E_v is the valence-band maximum, μ_e is the electron chemical potential (or Fermi energy) relative to E_v, n_s is the number of atoms of the chemical species s in the supercell, and μ_s is the atomic chemical potential of the species s. The values of E_v's for different supercells are aligned by using an average potential correction.[41]

III. MIGRATION OF OXYGEN COMPLEXES

A. Single interstitial oxygen atom

Figure 1 shows the calculated diffusive jump of a single O atom along the minimum-energy migration path. At the saddle point [Fig. 1(b)] the O atom is approximately three-fold coordinated. The corresponding configuration is called the "Y-lid" configuration, and the oxygen atom in this configuration is denoted by O_y. The calculated saddle-point energy is 2.3 eV (2.57 eV for a C_{2v}-symmetric structure) in close agreement with the experimental value of 2.54 eV (Ref. 3) and with the earlier calculated values of 2.2–2.5 eV (Refs. 25–29) given in Table I. The diffusing O atom can practically migrate in any $[1\bar{1}0]$ direction because the calculated rotation barrier of O_i between the six minima around the Si-Si axis is only 50 meV (the earlier estimate given in Ref. 41 is 20 meV).

TABLE I. Calculated migration energies for small oxygen complexes. Our migration energies are for neutral complexes. The unit of energy is eV.

	Present	Snyder et al.[a]	Ewels et al.[b]	Ramamoorthy and Pantelides[c]	Coutinho et al.[d]
O_i	2.3	2.49	2.5	2.2	2.2
O_{2i} via O_{2r}	0.95	1.36			
O_{2i} via distorted O_{2r}	1.8		2.4	1.5	1.4
O_{2i} via O_i-O_y	2.17		1.1–1.5		1.6
O_{2i} via skewed O_i-Si-Si-O_i	2.34				2.2
O_3 chain via O_{2r}	0.68				
non-(110) O_3	$\geq$2.3				
O_4 chain via O_{2r}	0.65				
non-(110) O_4	$\geq$2.3				

[a]Reference 25.
[b]Reference 26.
[c]References 27 and 28.
[d]Reference 29.
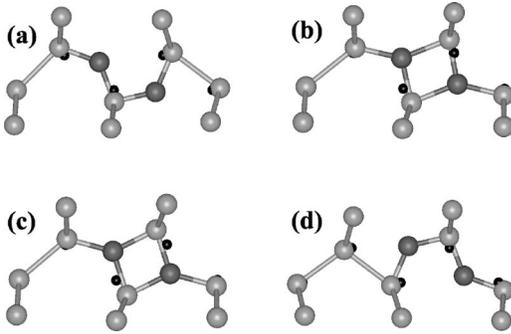
FIG. 2. Calculated correlated transfer of an electrically neutral O_2 via O_{2r}. Black and grey balls represent oxygen and silicon atoms, respectively. Black dots denote the equilibrium positions of the silicon atoms. (a) Staggered O_2 (O_{2i}) in the (110) plane. (b) Saddle-point configuration. (c) O_{2r}. (d) Final O_{2i}. (e) Rotated O_{2i} for the rest half-step. The structures for O_2^{++} are almost identical.

B. Oxygen dimer complexes

The minimum-energy migration paths of O_2 are more complex than those of O_i. We have studied the following cases: (i) the migration of O_2 via an intermediate four-membered ring (O_{2r}) configuration[25] [see Fig. 2(c)], (ii) the migration of O_2 through a saddle-point configuration with one oxygen atom in a bond center and the other in a Y-lid position (O_i-O_y),[26] and (iii) the migration of O_2 via a skewed O_i-Si-Si-O_i structure.[40] The calculated migration energies, defined as the difference between the maximum and minimum values of the formation energy, are summarized in Table I together with the results from other calculations.

We find that the calculated minimum-energy migration path of an electrically neutral O_2 proceeds via O_{2r}. As shown in Fig. 2, the two O atoms move in concert as follows: The staggered O_2 (O_{2i}) [Fig. 2(a)] → saddle-point O_2 (nearly O_{2r}) [Fig. 2(b)] → O_{2r} [Fig. 2(c)] → saddle-point O_2 → O_{2i} [Fig. 2(d)]. To continue migration in the same $[1\bar{1}0]$ direction, each O atom in O_{2i} [Fig. 2(d)] should be rotated by π around its Si-Si axis to give the configuration of Fig. 2(e). The calculated rotation barrier is less than 0.1 eV which is less than the calculated migration energy of 0.98 eV (Table I).

The calculated formation energy for an electrically neutral O_2 migrating via O_{2r} is shown as a function of the reaction coordinate X in Fig. 3 (diamonds). The energy has a local minimum C at O_{2r} [Fig. 2(c)] which is thus a metastable structure. This result agrees qualitatively with the empirical MINDO/3 calculation by Snyder *et al.*[25] However, quantitatively we find a much shallower valley: 0.06 vs 1.3 eV. Other first-principles calculations by Ewels *et al.*,[26] Ramamoorthy and Pantelides,[28] and Coutinho *et al.*[29] do not find any metastable O_{2r} structure but report only a single saddle point. An explanation for this difference may be as follows. It appears from the figures in Refs. 28 and 29 that their O_{2r} structures in the migration paths differ from our O_{2r} structure [Fig. 2(c)]. This may imply that their migration paths do not pass through the actual minimum-energy configuration. In fact, we find, using a nearby migration path, only a single saddle-point maximum with an energy of 1.8 eV which is close to
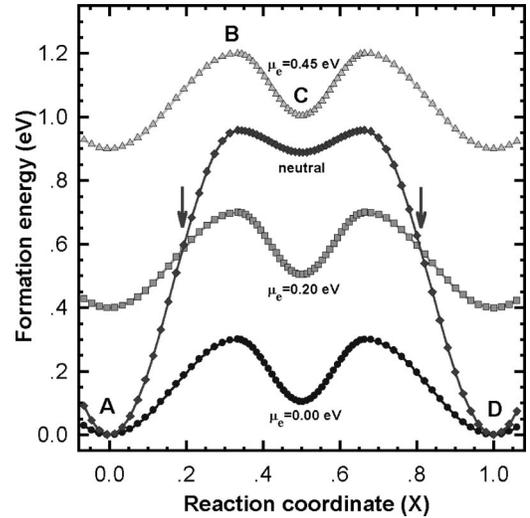
FIG. 3. Calculated formation energies as a function of the reaction coordinate X for the migration of O_2 via O_{2r}. Circles, squares, and triangles represent formation energies in a doubly positive charge state for $\mu_e = 0.0$, 0.20, and 0.45 eV, respectively. Diamonds represent formation energies in a neutral charge state. Arrows denote the charge state changes for $\mu_e = 0.35$ eV. A–D correspond to the configurations of Figs. 2(a)–2(d), respectively. The energies are calculated with respect to the energy of the neutral O_{2i} at $X = 0.0$.

the values of 1.5 and 1.4 eV obtained in Refs. 28 and 29, respectively (Table I). O_{2r} [Fig. 2(c)] is a metastable double donor. However, the calculated formation energy of O_{2r} is 0.89 eV higher than that of O_{2i} indicating that the equilibrium concentration of O_{2r} probably lies below the detection limit.

As to the dependence of the formation energy on the charge state $(0, +, \text{ or } ++)$ all calculated O_2 structures are found to exhibit negative-U behavior. The formation energies of the singly positively charged structures are therefore omitted in Fig. 3. As shown in Fig. 3 the formation energy of O_2^{++} depends on μ_e but that of the neutral O_2 does not [$Q = 0$ in Eq. (3)]. At $X = 0.0$ the neutral O_{2i} [Fig. 2(a)] has always a lower formation energy for $\mu_e > 0.0$ eV and is thus stabler than O_2^{++}. For a migrating O_2 [X increases from 0 to 1 when O_2 visits the structures in Figs. 2(a)–2(d)] the migration energy is defined as the difference between the maximum and minimum formation energies in Fig. 3. In n-type silicon with $\mu_e \geq 0.33$ eV the maximum $X = 0.03$ of the neutral formation energy curve (diamonds in Fig. 3) lies below the corresponding maximum B of the doubly positive one (triangles in Fig. 3). Thus, in this case the calculated migration energy is 0.95 eV. In ideal p-type silicon with $\mu_e = 0.0$ eV, O_2 migrates in the doubly positive charge state because O_2^{++} (circles in Fig. 3) is stabler than the neutral O_2 (diamonds in Fig. 3) for all values of $X(0 < X < 1)$. In this case the migration energy is 0.3 eV which is significantly lower than the previous value of 0.95 eV. For $0.0 < \mu_e < 0.33$ eV the maximum B of the doubly positive formation energy curve (squares in Fig. 3) lies below that of the neutral one (diamonds in Fig. 3) and thus determines the migration energy. For example, for $\mu_e = 0.2$ eV O_2 migrates first in

the electrically neutral state for $0.0 < X < 0.2$ (diamonds in Fig. 3), then in a doubly positive state for $0.2 < X < 0.8$ (squares in Fig. 3), and finally again in the neutral state for $0.8 < X < 1.0$ (diamonds in Fig. 3). This is the charge-exchange-assisted diffusion mechanism. The calculated migration energy is 0.7 eV for $\mu_e = 0.2$ eV and the effect of the charge-exchange mechanism is to lower the migration energy below the value of 0.95 eV in n-type silicon.

We find that migration of O_2 via O_i-O_y is not energetically favorable in contrast to the calculations by Ewels *et al.*[26] and Coutinho *et al.*[29] (Table I). We also find, in agreement with Coutinho *et al.*,[29] that the migration of O_2 via the skewed O_i-Si-Si-O_i configuration has a high migration energy of 2.34 eV (Table I). Both O_i-O_y and O_i-Si-Si-O_i have defect levels close to the valence-band maximum and no charge exchange from neutral to doubly positive occurs despite the fact that one of the O atoms appears as threefold coordinated during the diffusive jump. This resembles the diffusive jump of O_i where O_i remains neutral though it passes a threefold coordinated saddle-point configuration [see Fig. 1(b)].

We find that O_{2i} may reorient to a new $[1\bar{1}0]$ direction by the following mechanism: $O_{2i} \rightarrow$ distorted O_{2r} out of the original (110) plane $\rightarrow O_{2i}$ in the new $[1\bar{1}0]$ direction. The calculated reorientation energy is 2.1 eV, which is about the same as the calculated migration energy of 2.3 eV for the diffusive jump of O_i (Table I). Also the correlated transfer via the skewed O_i-Si-Si-O_i configuration mentioned above results in a reoriented O_{2i} with a slightly higher reorientation energy of 2.34 eV (Table I). The calculated values of 2.1 and 2.34 eV compare favorably with the experimental reorientation energy of 2.5 eV for the well-oxygen-dispersed silicon.[46-48]

C. Oxygen trimer complexes

A fast-diffusing O_2 may capture an O_i within the capture radius (typically 5–8 Å). We use the same capture radius of 5 Å in all our calculations. Figure 4 shows the silicon lattice in the $[1\bar{1}0]$ direction along which O_2 is migrating and the bond centers within the capture radius of 5 Å labeled from A to F, according to the increasing distance from the $[1\bar{1}0]$ axis. Figure 5 shows the corresponding calculated trimer complexes [Figs. 5(a)–5(f)] that result when the migrating O_2 captures an O_i at (A)–(F), respectively.

The calculated binding energies between O_{2i} and O_i in the straight chain structure of Fig. 5(a), called the O_3 chain in the following, and in the branched structure of Fig. 5(b) are 0.31 and 0.23 eV, respectively, and in the rest of the branched structures of Figs. 5(c)–5(f) 0.01–0.06 eV. (We call a structure which consists of a straight chain and a side O_i a branched structure or a branched chain.) The total number of bond sites C–F in Fig. 4 is larger than that of bond sites B and A, the ratios being 10:2:1, respectively. Notice that two adjacent bonds of types A, D, and E fit within one period of $2^{-1/2}a$ in the $[1\bar{1}0]$ direction but only one bond of types B, C, and F fits. The probabilities for the formation of the O_3 chain [Fig. 5(a)], the structure [Fig. 5(b)], and the structures
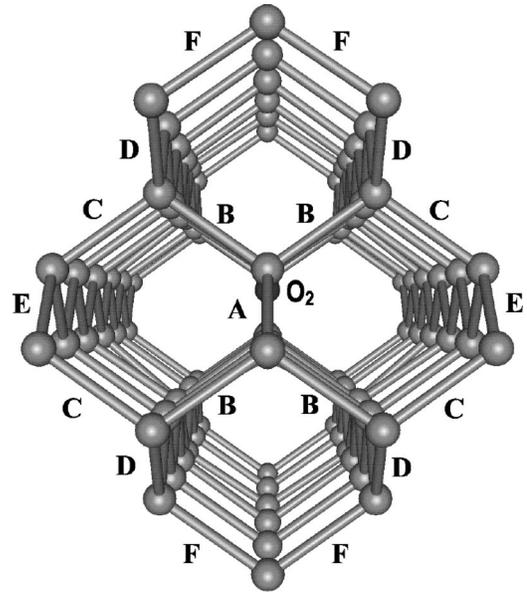
FIG. 4. Bond sites within the assumed capture radius of 5 Å from the migration axis. Black balls represent the oxygen atoms of an oxygen dimer migrating in the $[1\bar{1}0]$ direction normal to the plane of the paper. Grey balls represent silicon atoms.

in Figs. 5(c)–5(f) are thus 1/13, 2/13, and 10/13, respectively. The migration energies of the structures in Figs. 5(c)–5(f) are more than 2.3 eV (Table I) which makes their migration less important. However, their inclusion is important because they increase through restructuring the concentration of O_3 chains that have a low migration energy of 0.68 eV (Table I) and are responsible for the migration of trimer complexes.
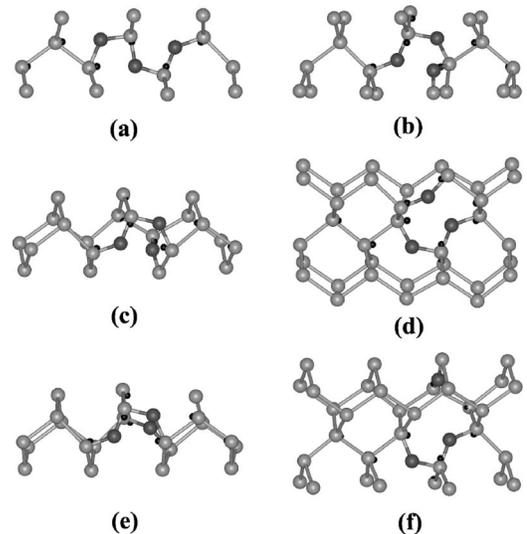
FIG. 5. Calculated oxygen trimer structures that result when an O_{2i} migrating along the $[1\bar{1}0]$ axis captures an O_i. The resulting structures are dependent on the relative position of O_i such that the structures (a)–(f) result from the capturing of O_i in the bond sites A–F in Fig. 4, respectively. Black and grey balls represent oxygen and silicon atoms, respectively. Black dots denote the equilibrium positions of the silicon atoms.
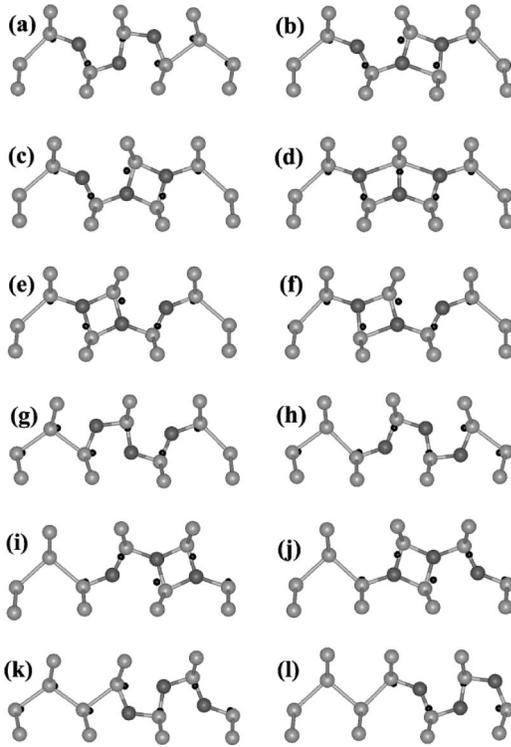
FIG. 6. Calculated correlated transfer of a neutral O_3 chain. Black and grey balls represent oxygen and silicon atoms, respectively. Black dots denote the equilibrium positions of the silicon atoms. (a) Initial staggered O_3 chain. (b) Saddle-point configuration. (c) Intermediate O_i-O_{2r} configuration. (d) Saddle-point configuration. (e) Intermediate O_{2r}-O_i configuration. (f) Saddle-point configuration. (g) Half-way staggered O_3 chain. (h) Rotated O_3 chain for the second half of the correlated transfer. (i) Intermediate O_i-O_{2r} configuration. (j) Intermediate O_{2r}-O_i configuration. (k) Staggered O_3 chain. (l) Final rotated staggered O_3 chain. Electron chemical potential $\mu_e \geqslant 0.48$ eV.

The calculated correlated transfer of an electrically neutral O_3 chain along the minimum-energy migration path is shown in Fig. 6 and the corresponding formation energy curve as a function of the reaction coordinate X in Fig. 7 (diamonds). Likewise to O_2, the correlated transfer of the O_3 chain occurs via O_{2r} structures: the staggered O_3 chain [Fig. 6(a)] is transformed via a saddle-point configuration [Fig. 6(b)] to O_i-O_{2r} [Fig. 6(c)], then over the C_{2v}-symmetric O_{3r} configuration [Fig. 6(d)] to O_{2r}-O_i [Fig. 6(e)], and next to the staggered O_3 chain [Fig. 6(g)]. To complete the correlated transfer in the same $[1\bar{1}0]$ direction, each oxygen atom of the O_3 chain in Fig. 6(g) should be rotated by π around its Si-Si axis into the configuration shown in Fig. 6(h). Next, the staggered O_3 chain [Fig. 6(h)] is transferred to O_i-O_{2r} [Fig. 6(i)], then via the C_{2v}-symmetric O_{3r} configuration to O_{2r}-O_i [Fig. 6(j)], and then to the staggered O_3 chain [Fig. 6(k)]. The rotation by π of each O atom around its Si-Si axis brings the O_3 chain into the final staggered form of Fig. 6(l) which corresponds exactly to the initial staggered configuration shifted by $2^{-1/2}a$ in the $[1\bar{1}0]$ direction. The calculated rotational barrier is less than 0.25 eV and thus less than the calculated migration energy of 0.68 eV (Table I).
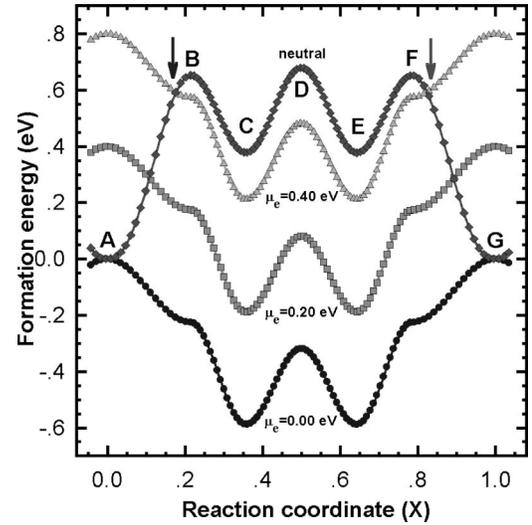
FIG. 7. Calculated formation energies as a function of the reaction coordinate X for the correlated transfer of the O_3 chain. Circles, squares, and triangles represent formation energies in a doubly positive charge state for $\mu_e = 0.0$, 0.2, and 0.4 eV, respectively. Diamonds represent formation energies in a neutral charge state. Arrows denote the charge state changes for $\mu_e = 0.4$ eV. A–G correspond to the configurations of Figs. 6(a)–6(g), respectively. The energies are calculated relative to the energy of the neutral O_3 chain at $X = 0.0$.

As shown in Fig. 7, the formation energy of the O_3 chain depends on μ_e. In n-type silicon with $\mu_e \geqslant 0.48$ eV the electrically neutral O_3 chain is the stablest (diamonds in Fig. 7) among the relevant charge states (0, $+$, and $++$) in the whole range $0.0 < X < 1.0$. Thus, the O_3 chain migrates solely in the neutral charge state. The calculated migration energy is 0.68 eV in this case. In ideal p-type silicon with $\mu_e = 0.0$ eV the doubly positive O_3^{++} chain is the stablest in the whole range $0.0 < X < 1.0$ (circles in Fig. 7). In this case the O_3 chain migrates solely in the doubly positive charge state and the calculated migration energy is 0.60 eV. For $0.0 < \mu_e < 0.48$ eV the migration of the O_3 chain is influenced by the charge-exchange mechanism. For example, for $\mu_e = 0.4$ eV the O_3 chain migrates first in the neutral state for $0.0 < X < 0.17$ (diamonds in Fig. 7), then in the doubly positive state for $0.17 < X < 0.84$ (triangles in Fig. 7), and finally again in the neutral state for $0.84 < X < 1.0$ (diamonds in Fig. 7). In this case the calculated migration barrier is 0.60 eV which is less than the value of 0.68 eV in n-type silicon. For $\mu_e = 0.2$ eV the migration barrier is lowered further below 0.5 eV by the charge-exchange mechanism [diamonds (0) $\rightarrow$ squares ($++$) $\rightarrow$ diamonds (0) in Fig. 7].

The O_3 structures in Figs. 5(b)–5(f) which do not belong to the (110) plane of O_{2i} have distinctly higher migration energies of $\geqslant 2.3$ eV compared with the migration energy of only 0.68 eV of the neutral O_3 chain (Table I). This is mainly due to the fact that the O atom located out of the (110) plane of O_{2i} must migrate similarly to a single O_i. However, the presence of the O_3 structures in Figs. 5(b)–5(f) is important because they increase significantly the concentration of easily migrating O_3 chains through restructuring. The calculated
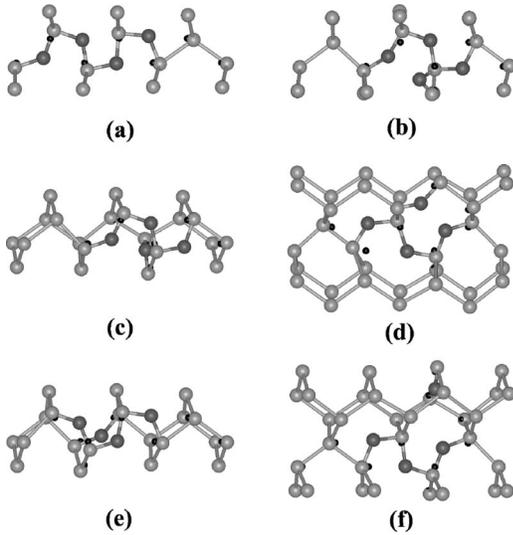
FIG. 8. Calculated oxygen tetramer structures that result when an O_3 chain migrating along the $[1\bar{1}0]$ axis captures an interstitial oxygen. Black and grey balls represent oxygen and silicon atoms, respectively. Black dots denote the equilibrium positions of the silicon atoms. The resulting structures are dependent on the relative position of O_i such that the structures (a)–(f) result from the capturing of O_i in the bond sites A–F in Fig. 4, respectively.

restructuring energies for the complexes in Fig. 5 are as follows: Fig. 5(b) → 5(a) 1.9 eV; Fig. 5(a) → 5(b) 1.98 eV; Fig. 5(c) → 5(b) and 5(d) → 5(b) 2.3 eV; Fig. 5(c) → 5(d), 5(c) → 5(e), and 5(f) → 5(d) 2.5 eV. These restructuring energies do not depend on μ_e.

The restructuring of the O_3 structure in Fig. 5(b) may also result in a reoriented O_3 chain. The mechanism for this is as follows: O_{2i}-$O_{i,out}=O_i$-$O_{2i,new}\rightarrow O_y$-$O_{2i,new}\rightarrow O_{3,new}$ chain ["out" means out of the original (110) plane and "new" means in the new $[1\bar{1}0]$ direction]. The calculated reorientation energy is 1.9 eV which agrees closely with the experimental values of 1.8–1.96 eV for the heat-treated samples.[46–48]

The electrically inactive staggered O_3 chain and the electrically active O_i-O_{2r} (and O_{2r}-O_i) form a bistable system. A similar bistable system is also found experimentally for TDD0.[49] This similarity led us to identify O_i-O_{2r} (and O_{2r}-O_i) as TDD0.[42,43]

D. Oxygen tetramer complexes

Since the concentration of O_i is always by three orders of magnitude (or more) higher than that of any other oxygen complex, the formation of O_4 by the association of two oxygen dimers is far less important than the reaction $O_3+O_i \rightarrow O_4$. Figure 8 shows the calculated O_4 structures that result when an O_3 chain migrating along the $[1\bar{1}0]$ axis captures an O_i. The binding energies between the neutral O_3 chain and O_i in the neutral O_4 chain of Fig. 8(a) and in the neutral structure of Fig. 8(b) are 0.55 and 0.14 eV, respectively. The corresponding binding energies in the neutral structures of Figs. 8(c)–8(f) are 0.01–0.04 eV.
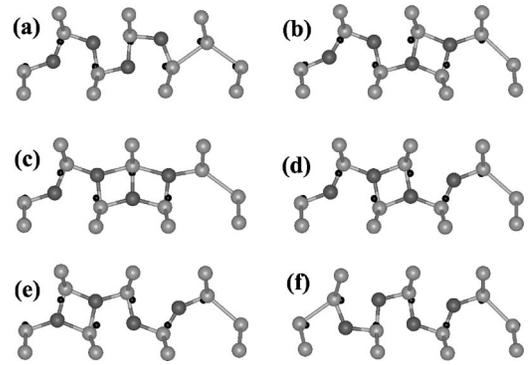
FIG. 9. Calculated correlated transfer of a neutral O_4 chain. Black and grey balls represent oxygen and silicon atoms, respectively. Black dots denote the equilibrium positions of the silicon atoms. (a) Initial staggered O_4. (b) Intermediate O_{2i}-O_{2r} configuration. (c) O_i-O_{3r} saddle-point configuration. (d) Intermediate O_i-O_{2r}-O_i configuration. (e) Intermediate O_{2r}-O_{2i} configuration. (f) Staggered O_4.

The calculated correlated transfer of a neutral O_4 chain along the minimum-energy migration path is shown in Fig. 9 and the corresponding formation energy curve as a function of the reaction coordinate X in Fig. 10 (diamonds). The correlated transfer of the O_4 chain in Fig. 9 resembles that of the O_3 chain: staggered O_4 chain [Fig. 9(a)] → O_{2i}-O_{2r} [Fig. 9(b)] → saddle-point O_i-O_{3r} [Fig. 9(c)] → O_i-O_{2r}-O_i [Fig. 9(d)] → O_{2r}-O_{2i} [Fig. 9(e)] → staggered O_4 chain [Fig. 9(f)]. To complete the correlated transfer in the $[1\bar{1}0]$ direction, each oxygen atom of the O_4 chain of Fig. 9(f) should be rotated by π around its Si-Si axis. We expect that
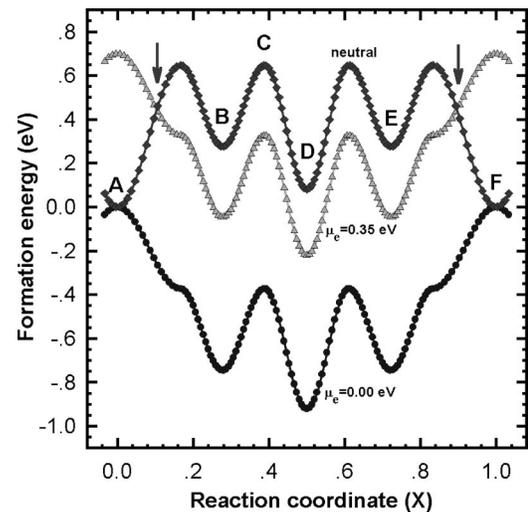
FIG. 10. Calculated formation energies as a function of the reaction coordinate X for the correlated transfer of the O_4 chain. Circles and triangles represent formation energies in a doubly positive charge state for $\mu_e=0.0$ and 0.35 eV, respectively. Diamonds represent formation energies in a neutral charge state. Arrows denote the charge state changes for $\mu_e=0.35$ eV. A–F correspond to the configurations of Figs. 9(a)–9(f), respectively. The energies are calculated relative to the energy of the neutral staggered O_4 chain at $X=0.0$.

the rotational barrier is less than the calculated migration energy of 0.65 eV (Table I).

As shown in Fig. 10, the calculated formation energy of the O_4 chain depends on the value of μ_e. In n-type silicon with $\mu_e \geqslant 0.51$ eV the electrically neutral O_4 chain is the stablest in the whole range $0.0 < X < 1.0$ (diamonds in Fig. 10). In this case the O_4 chain migrates solely in the neutral charge state and the calculated migration energy is 0.65 eV (Table I). In ideal p-type silicon with $\mu_e = 0.0$ eV the doubly positive O_4^{++} chain is the stablest in the whole range $0.0 < X < 1.0$ (circles in Fig. 10) and the O_4 chain migrates solely in the doubly positive charge state. In this case the migration energy is 0.91 eV. For $0.0 < \mu_e < 0.51$ eV the migration of the O_4 chain is influenced by the charge-exchange mechanism. For example, for $\mu_e = 0.35$ eV the O_4 chain migrates first in the neutral state for $0.0 < X < 0.1$ (diamonds in Fig. 10), then in the doubly positive state for $0.1 < X < 0.9$ (triangles in Fig. 10), and finally again in the neutral state for $0.9 < X < 1.0$ (diamonds in Fig. 10). In this case the calculated migration energy is 0.60 eV which is less than the value of 0.65 eV in n-type silicon.

The migration energies of the structures of Figs. 8(b)–8(f) exceed 2.3 eV (Table I) which makes their migration less important. However, their presence is important because they increase significantly the concentration of easily migrating O_4 chains through restructuring. The calculated activation energies for restructuring of O_4 chains are 2.2–2.5 eV, which are still consistent with the experimental values of 1.8–1.96 eV for the heat-treated samples.[46–48]

Figure 10 shows that the electrically active O_{2i}-O_{2r} (B) or O_{2r}-O_{2i} (E) and O_i-O_{2r}-O_i (D) structures form a bistable system with the electrically inactive staggered O_4 chain (A or F). A similar bistable system is found with the infrared absorption experiments for TDD1 and TDD2.[50,51] Figure 10 also shows that O_i-O_{2r}-O_i can be easily formed from O_{2i}-O_{2r} or O_{2r}-O_{2i}. An experimental kinetic study implies that TDD2 may form via restructuring from TDD1.[20] It is found experimentally that the TDD1 $\rightarrow$ (inactive) X state and the TDD2 $\rightarrow$ X-state barriers are 0.54 and 0.71 eV, respectively.[6,52] We find from Fig. 10 that the O_{2i}-O_{2r} (B) $\rightarrow O_4$-chain (A) and O_i-O_{2r}-O_i (D) $\rightarrow O_4$-chain (A) barriers are 0.36 and 0.50 eV, respectively, which, after adding the experimental difference from TDD^{++} to TDD^+ of 0.15 eV, agree closely with the experimental values. These comparisons led us to identify O_{2i}-O_{2r} (and O_{2r}-O_{2i}) as TDD1 and O_i-O_{2r}-O_i as TDD2.[42,43]

E. Oxygen pentamer complexes

The migration energies of the pentamer structures with five oxygen atoms are studied in the same way as the trimer and tetramer structures above. It is assumed that an O_4 chain migrating along the $[1\bar{1}0]$ direction captures an O_i (see Fig. 4). The calculated binding energy between the neutral O_4 chain and O_i is largest (0.86 eV) in the neutral C_{2v}-symmetric electrically active O_5 chain shown in Fig. 11(c) and slightly less (0.61 eV) in the neutral electrically inactive staggered O_5 chain shown in Fig. 11(a). All other
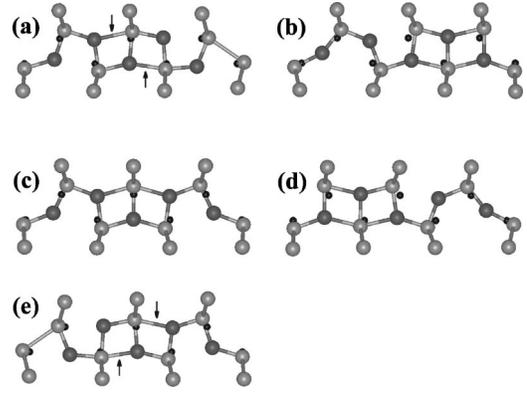
FIG. 11. Calculated correlated transfer of a neutral O_5 chain. Black and grey balls represent oxygen and silicon atoms, respectively. Black dots denote the equilibrium positions of the silicon atoms. Arrows show the longest bonds of the rings in staggered structures. (a) Initial staggered O_5. (b) Saddle-point O_{2i}-O_{3r}. (c) C_{2v}-symmetric O_i-O_{3r}-O_i. (d) Saddle-point O_{3r}-O_{2i}. (e) Half-way staggered O_5.

(branched) structures having the captured O_i out of the (110) plane of the O_4 chain have binding energies that are about 0.5 eV lower.

The calculated migration energy of the O_5 chain is 0.7–1.2 eV depending on the value of μ_e. It is significantly lower than the migration energies of 2.3–2.5 eV for the branched structures. Thus also in the case of pentamer structures, the O_5 chain is responsible for migration. However, also the branched pentamer structures mentioned must be included in the kinetic model because they increase significantly the concentration of O_5 chains through restructuring which takes place with activation energies of 2.3–2.5 eV.

The calculated correlated transfer of a neutral O_5 chain along the minimum-energy migration path is shown in Fig. 11 and the corresponding formation energy curve as a function of the reaction coordinate X in Fig. 12 (diamonds). The correlated transfer of the neutral O_5 chain in Fig. 11 proceeds similarly to those of the O_3 and O_4 chains. However, the structure of the O_5 chain in Fig. 11(a) corresponding to the staggered structure of the O_4 chain in Fig. 9(a) is no more so obviously staggered because it seems to contain two adjacent rings. It is still called staggered because (i) it is electrically inactive similarly to the earlier staggered structures, and (ii) elimination of the longest bond (marked with an arrow) in each ring reveals again the usual staggered structure. The correlated transfer of the neutral O_5 chain in Fig. 11 proceeds as follows: staggered O_5 chain [Fig. 11(a)] $\rightarrow$ saddle-point O_{2i}-O_{3r} [Fig. 11(b)] $\rightarrow O_i$-O_{3r}-O_i [Fig. 11(c)] $\rightarrow$ saddle-point O_{3r}-O_{2i} [Fig. 11(d)] $\rightarrow$ staggered O_5 chain [Fig. 11(e)]. To complete the correlated transfer in the same $[1\bar{1}0]$ direction, each oxygen atom of the O_5 chain in Fig. 11(e) should be rotated by π around its Si-Si axis. We expect that the rotational barrier is less than the calculated migration energy of 0.7 eV (Fig. 12, diamonds). Since the C_{2v}-symmetric O_5 chain in Fig. 11(c) is stabler than the staggered O_5 chain in Fig. 11(a) it would have been more natural to describe the correlated transfer as Fig. 5(c) $\rightarrow$5(d)$\rightarrow$5(e)$\rightarrow$ and so on.
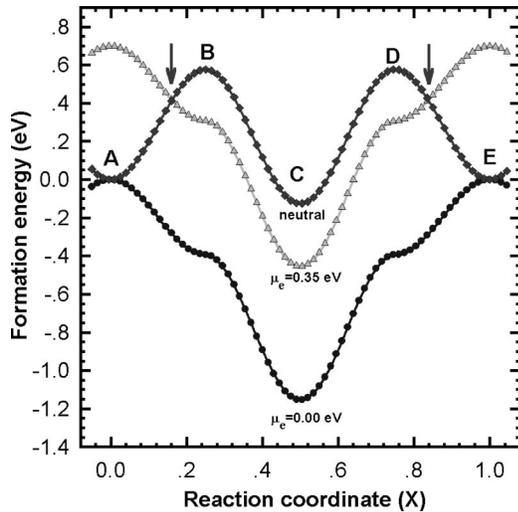
FIG. 12. Calculated formation energies as a function of the reaction coordinate X for the correlated transfer of the O_5 chain. Circles and triangles represent formation energies in a doubly positive charge state for $\mu_e = 0.00$ eV and $\mu_e = 0.35$ eV, respectively. Diamonds represent formation energies in a neutral charge state. Arrows denote the charge state changes for $\mu_e = 0.35$ eV. A–E correspond to the configurations of Figs. 11(a)–11(e), respectively. The energies are calculated relative to the energy of the neutral staggered O_5 chain at $X = 0.0$.

As shown in Fig. 12, the calculated formation energy of the O_5 chain depends on the value of μ_e. In n-type silicon with $\mu_e \geq 0.52$ eV the electrically neutral O_5 chain is the stablest in the whole range $0.0 < X < 1.0$ (diamonds in Fig. 12). In this case the O_5 chain migrates solely in the neutral charge state and the calculated migration energy is 0.7 eV. In ideal p-type silicon with $\mu_e = 0.0$ eV the doubly positive O_5^{++} chain is the stablest in the whole range $0.0 < X < 1.0$ (circles in Fig. 12) and the O_5 chain migrates solely in the doubly positive charge state. In this case the calculated migration energy is 1.2 eV. For $0.0 < \mu_e < 0.51$ eV the migration of the O_5 chain is influenced by the charge-exchange mechanism. For example, for $\mu_e = 0.35$ eV the O_5 chain migrates first in the neutral state for $0.0 < X < 0.16$ (diamonds in Fig. 12), then in the doubly positive state for $0.16 < X < 0.84$ (triangles in Fig. 12), and finally again in the neutral state for $0.84 < X < 1.0$ (diamonds in Fig. 12). The calculated migration energy is 0.8 eV in this case.

Since the electrically active O_5 chain in Fig. 11(c) has a lower formation energy than the electrically inactive staggered O_5 chain in Fig. 11(a) (see Fig. 12) the bistability met in the cases of the O_3 and O_4 chains disappears here. It is found experimentally that TDD3 does not display bistability.[50,51] This comparison led us to identify the O_i-O_{3r}-O_i chain structure [Fig. 11(c)] as TDD3.[42,43]

F. Large O_n ($6 \leq n \leq 13$) complexes

The correlated transfers of the large O_n chains ($6 \leq n \leq 13$) are similar to the transfer of the O_5 chain above. As an example, the calculated structures of a neutral O_{10} chain along the minimum-energy path are shown in Fig. 13 and the
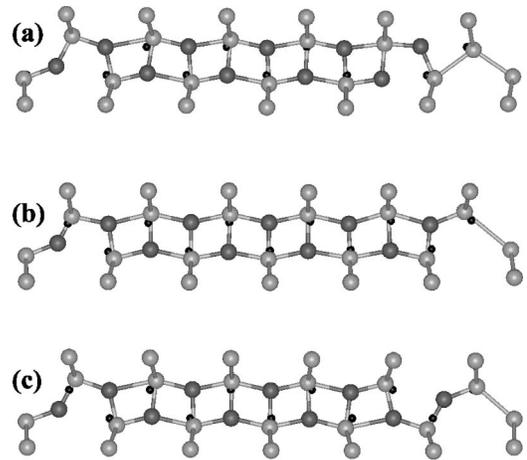
FIG. 13. Calculated correlated transfer of a neutral O_{10} chain. Black and grey balls represent oxygen and silicon atoms, respectively. Black dots denote the equilibrium positions of the silicon atoms. (a) Staggered O_{10} [cf. Fig. 11(a)]. (b) Saddle-point configuration O_i-O_{9r}. (c) O_i-O_{8r}-O_i.

corresponding formation energy as a function of the reaction coordinate X is shown in Fig. 14 (diamonds). The correlated transfer of the neutral O_{10} chain (Fig. 13) proceeds as follows: staggered O_{10} chain [Fig. 13(a)] $\rightarrow$ saddle-point O_i-O_{9r} [Fig. 13(b)] $\rightarrow O_i$-O_{8r}-O_i [Fig. 13(c)] $\rightarrow$ saddle-point O_{9r}-$O_i\rightarrow$ staggered O_{10} chain. To complete the correlated transfer each O atom of the O_{10} chain must be rotated by π around its Si-Si axis. We expect that the rotational barrier still remains less than the migration energy of about 2.0 eV (Fig. 14). Since the O_i-O_{8r}-O_i chain in Fig. 13(c) is stabler
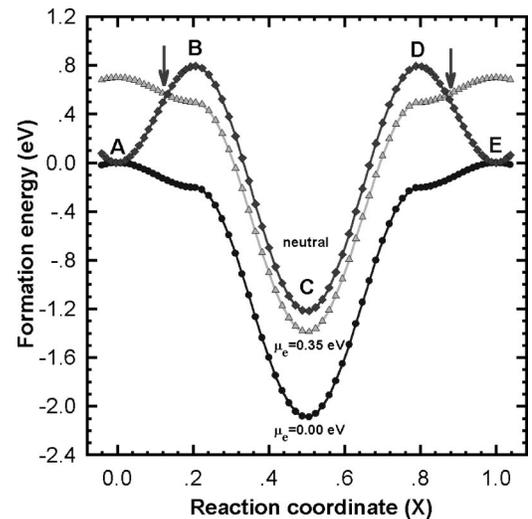
FIG. 14. Calculated formation energies as a function of the reaction coordinate X for the correlated transfer of the O_{10} chain. Circles and triangles represent formation energies in a doubly positive charge state for $\mu_e = 0.0$ eV and $\mu_e = 0.35$ eV, respectively. Diamonds represent formation energies in a neutral charge state. Arrows denote the charge state changes for $\mu_e = 0.35$ eV. A–C correspond to the configurations of Figs. 13(a)–13(c), respectively. The energies are measured relative to the energy of the neutral staggered O_{10} chain at $X = 0.0$.
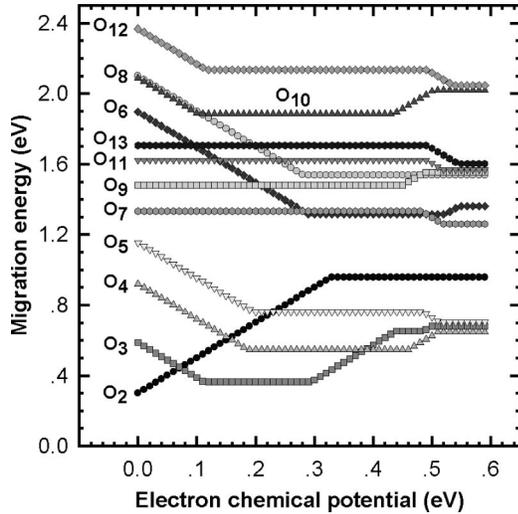
FIG. 15. Calculated migration energies of oxygen chains as a function of the electron chemical potential μ_e.

than the staggered O_{10} chain in Fig. 13(a) it would have been more natural to describe the correlated transfer starting from the O_i-O_{8r}-O_i chain.

As shown in Fig. 14 the calculated formation energy of the O_{10} chain depends on the value of μ_e. In n-type silicon with $\mu_e \geq 0.5$ eV the electrically neutral O_{10} chain is the stablest form in the whole range $0.0 < X < 1.0$ (diamonds in Fig. 14). In this case the O_{10} chain migrates solely in the neutral charge state and the calculated migration energy is 2.0 eV. In ideal p-type silicon with $\mu_e = 0.0$ eV the doubly positive O_{10}^{++} chain is the stable form in the whole range $0.0 < X < 1.0$ (circles in Fig. 14) and the O_{10} chain migrates solely in the doubly positive charge state. In this case the calculated migration energy is 2.1 eV. For $0.0 < \mu_e < 0.5$ eV the migration of the O_{10} chain is influenced by the charge-exchange mechanism. For example, for $\mu_e = 0.35$ eV the O_{10} chain migrates first in the neutral state for $0.0 < X < 0.12$ (diamonds in Fig. 14), then in the doubly positive state for $0.12 < X < 0.88$ (triangles in Fig. 14), and finally again in the neutral state for $0.88 < X < 1.0$ (diamonds in Fig. 14). The calculated migration energy is 1.9 eV in this case. The migration energies of the large O_n chains ($6 \leq n \leq 10$) are still relatively low (1.3–2.0 eV) and the inclusion of these chains in the kinetic model is essential. Analogously to the O_i-O_{3r}-O_i structure of the O_5 chain the electroactive O_i-O_{nr}-O_i structures of the large chains were identified as TDDn ($n = 4$–7).[42,43]

IV. ENERGIES AND REACTIONS

A. Migration energies and association reactions

The calculated migration energies E_m, given in Fig. 15, depend on μ_e. The migration energies for the short oxygen chains (O_{2i}–O_5) are only 0.3–1.2 eV, which are much less than the migration energy of O_i (2.3 eV). Even the longest chains have migration energies less than 2.3 eV. This indicates that migration of all oxygen chains should be included in the kinetic model, not only that of O_{2i}. Thus, we expect

TABLE II. Calculated formation energies (in eV). n denotes the number of oxygen atoms. E_f^x, E_f^a, and E_f^b denote the formation energies of an electrically inactive (staggered) chain, of a ring-type electrically active TDD chain, and of a non-(110)-planar complex shown in Figs. 5(b) and 8(b). E_f^a is given for the neutral (0) and doubly positive ($++$) charge states at $\mu_e = 0$. The μ_e dependence of E_f^a can be obtained from the equation $E_f^a(Q, \mu_e) = E_f^a(Q, 0) + Q \cdot \mu_e$ [see Eq. (3)]. In the case $n = 4$ the values of $E_f^a(0)$ and $E_f^a(++)$ are given for O_i-O_{2r}-O_i (TDD2). E_f^{c-} denotes the average formation energy of the non-(110)-planar complexes shown in Figs. 5(c)–5(f) and 8(c)–8(f). The O_1–O_5, O_6–O_8, and O_9–O_{14} chains are calculated with the cubic 128, elongated 108, and elongated 162 atom-site supercells, respectively.

n	E_f^x	$E_f^a(0)$	$E_f^a(++)$	E_f^b	E_f^{c-}
1	1.10				
2	1.99	2.88	2.10	2.09	2.29
3	2.77	3.15	2.19	2.98	3.03
4	3.31	3.40	2.39	3.73	3.84
5	3.80	3.68	2.65	3.95	4.06
6	3.99	3.14	2.09	4.17	4.28
7	4.15	4.01	2.97	4.24	4.35
8	5.04	4.01	2.94	4.20	4.30
9	5.41	5.06	4.07	5.49	5.59
10	6.31	5.12	4.10	5.45	5.54
11	6.49	6.02	4.98		
12	7.41	6.11	5.04		
13	7.56	7.15	6.06		
14	8.51	7.25	6.14		

that the main association reactions proceed consecutively such that the migrating O_n chains *capture* the slowly moving but abundant O_i's:

$$O_i + O_i \rightarrow O_2,$$

$$O_2 + O_i \rightarrow O_3,$$

$$O_3 + O_i \rightarrow O_4,$$

$$O_4 + O_i \rightarrow O_5,$$

$$O_5 + O_i \rightarrow O_6,$$

$$O_6 + O_i \rightarrow O_7. \tag{4}$$
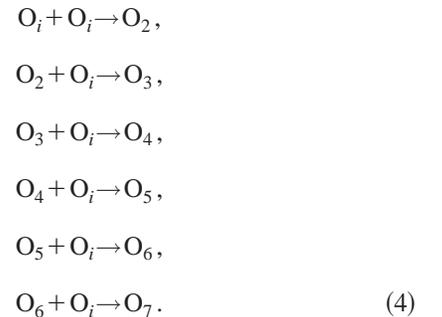
This is similar to the alternative suggested recently by Murin and Markevich for the formation of TDD's.[22]

B. Restructuring

The branched O_n complexes have high migration energies of ≥ 2.3 eV and have a tendency to restructure into the corresponding straight O_n chains which have lower formation energies. This can be seen from the calculated formation energies summarized in Table II. In the restructuring process the foremost captured O atom is transferred via threefold coordinated saddle point(s) to the chain aligning position. These processes resemble the diffusing jump of a single migrating O_i. The calculated restructuring energies are 2.1–2.3
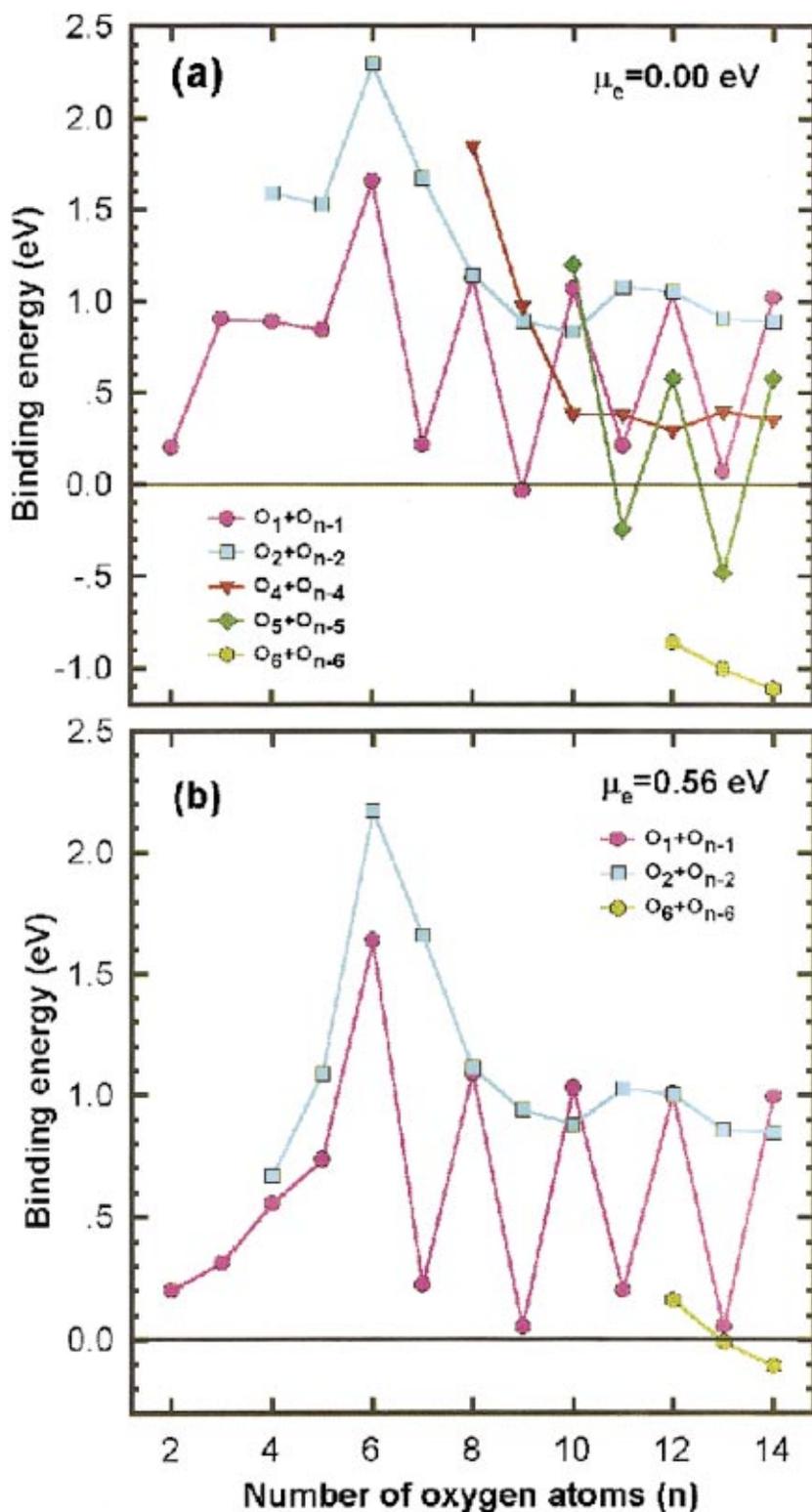
FIG. 16. (Color) Calculated smallest binding energies for the dissociation reactions as a function of n for the electron chemical potential $\mu_e = 0.0$ eV (a) and $\mu_e = 0.56$ eV (b).

eV for O_2 complexes, 1.9–2.5 eV for branched O_3 chains, 2.2–2.5 eV for branched O_4 chains, and 2.3–2.5 eV for branched O_5 chains. The last values of 2.3–2.5 eV are used also for larger branched $O_6–O_{16}$ chains in our kinetic simulations.[30] The calculated restructuring energies do not depend much on the value of the electron chemical potential μ_e. The results of our kinetic simulations do not depend sensitively on the detailed values of restructuring energies because simulations using one and the same value of 2.5 eV for all restructuring energies give virtually identical results.[30]

C. Binding energies and dissociation reactions

The dissociation of O_n chains into two fragments may occur in several ways. For example, for the O_8 chain we have the following possibilities:

$$O_8 \rightarrow O_i + O_7,$$

$$O_8 \rightarrow O_{2i} + O_6,$$

$$O_8 \rightarrow O_3 + O_5,$$

$$O_8 \rightarrow O_4 + O_4. \tag{5}$$
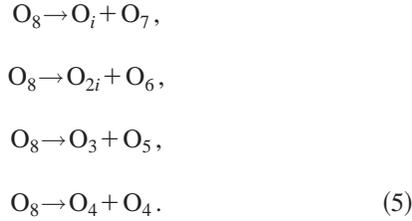
The dissociation reactions of the nonchain complexes have a larger number of possible reactions. The binding energies describing the tendency of an oxygen chain to dissociate into fragments can be calculated from their formation energies (Table II) using the equation

$$E_b^{lm}(\mu_e) = E_f^l(\mu_e) + E_f^m(\mu_e) - E_f^{l+m}(\mu_e), \tag{6}$$

where E_b^{lm} denotes the binding energy between the O_l and O_m chains in the straight O_{l+m} chain and E_f^l the lowest formation energy for the O_l chain among the 0 and $++$ charge states at the given μ_e value. The calculated binding energies for the energetically most favorable fragmentation reactions are shown for ideal p-type ($\mu_e = 0.0$ eV) and n-type ($\mu_e = 0.56$ eV) silicon in Figs. 16(a) and 16(b), respectively.

The basic dissociation mechanism is of the type $O_n \rightarrow O_i + O_{n-1}$, i.e., one of the outermost O_i's is ejected. This reaction type is dominating for $n \leqslant 9$ for all relevant values of μ_e though for $n = 9$ and for low values of μ_e [see Fig. 16(a)] the O_9 chain is no more stable but dissociates spontaneously to O_i and O_8. Also, at $n = 8$ the fragmentation $O_8 \rightarrow O_{2i} + O_6$ is energetically almost as favorable as $O_8 \rightarrow O_i + O_7$ for all relevant values of μ_e. In n-type silicon ($\mu_e = 0.56$ eV) for $n = 10$ the former fragmentation type, i.e., $O_{10} \rightarrow O_{2i} + O_8$, becomes most favorable, and for $n = 11$ the latter fragmentation type, i.e., $O_{11} \rightarrow O_i + O_{10}$, is again most favorable [Fig. 16(b)]. In n-type silicon for $n = 12$ the fragmentation $O_{12} \rightarrow O_6 + O_6$ dominates due to the high relative stability of O_6, and for the same reason O_{13} and O_{14} become unstable for the spontaneous dissociation to $O_6 + O_7$ and $O_6 + O_8$, respectively [Fig. 16(b)].

In n-type silicon ($\mu_e = 0.56$ eV) the calculated binding energies of the dissociation $O_n \rightarrow O_i + O_{n-1}$ first increase from 0.2 until 1.6 eV for $n = 2-6$ and then decrease [Fig. 16(b)]. This behavior resembles that found by Ourmazd et al.[53] by combining their kinetic model with experiments: their binding energies increase from 0.16 eV to 0.73 eV for $n = 2-5$ and then decrease.

D. Prefactors

Diffusion plays a central role in both the association and dissociation processes of our kinetic model.[30] The diffusion constants are given by

$$D = A_m \cdot \exp(-E_m/k_B T), \tag{7}$$

where the main temperature dependence is through the exponential factor. The prefactor A_m can be calculated using the transition-state theory[54,55] or *ab initio* molecular dynamics.[56] According to the transition-state theory A_m is of the general form[54,55]

$$A_m = C_m \cdot \exp(\Delta S/k_B), \tag{8}$$

where C_m is a constant and ΔS is the change in the vibrational entropy when the oxygen chain moves from its initial position to the saddle point. The ΔS factor in Eq. (8) is difficult to compute. Another, more direct way would be to evaluate A_m from $D(T)$ using constant-T *ab initio* molecular dynamics at high temperatures. In our case both ways are computationally too demanding. Therefore, in our kinetic model we have used the experimental values for the prefactors A_m of the first O_k chains ($k = 1-4$).[30] Since there is probably an "entropic bottleneck" which will increasingly hinder the motion of the longer O_k chains ($k > 4$), the diffusivities are geometrically suppressed for longer chains.[30] During the annealing the system is not in equilibrium, and thus configurational entropy is not well defined.

V. CONCLUSIONS

Migration, restructuring, and dissociation energies of oxygen complexes in silicon have been calculated using density-functional pseudopotential calculations in the local-density approximation. We find that the stablest oxygen complexes are straight chains, which also have the lowest migration energies. The calculated migration energies decrease from 2.3 eV for an interstitial oxygen atom (O_i) to low values of 0.4–1.6 eV for O_2–O_9 chains and 1.9–2.2 eV for longer chains. The oxygen chains (and thermal double donors) are expected to grow such that the migrating oxygen chains capture less-mobile but abundant O_i's: $O_n + O_i \rightarrow O_{n+1}$. The calculated energies for restructuring of branched oxygen chains into straight oxygen chains are 1.9–2.5 eV. It is expected that restructuring increases significantly the concentration of easily migrating chains. We also find that the O_2–O_9 chains dissociate energetically most favorably by ejecting one of the outermost oxygen atoms.

[1] *Early Stages of Oxygen Precipitation in Silicon*, edited by R. Jones (Kluwer Academic Publishers, Dordrecht, 1996).

[2] J.W. Corbett, R.S. Mac Donald, and G.D. Watkins, J. Phys. Chem. Solids **25**, 873 (1964).

[3] J.C. Mikkelsen, in *Oxygen, Carbon, Hydrogen, and Nitrogen in Crystalline Silicon*, edited by J. C. Mikkelson, Jr., S. J. Pearton, J. W. Corbett, and S. J. Pennycook, Mater. Res. Soc. Symp. Proc. 59 (Materials Research Society, Pittsburgh, 1986), p. 19.

[4] A. Borghesi, B. Pivac, A. Sassella, and A. Stella, J. Appl. Phys. **77**, 4169 (1995).

[5] C.S. Fuller, J.A. Ditzenberger, N.B. Hannay, and E. Buehler, Phys. Rev. **96**, 833 (1954).

[6] P. Wagner and J. Hage, Appl. Phys. A: Solids Surf. **A49**, 123 (1989).

[7] W. Götz, G. Pensl, and W. Zulehner, Phys. Rev. B **46**, 4312 (1992).

[8] H. Navarro, J. Griffin, J. Weber, and L. Genzel, Solid State Commun. **58**, 151 (1986).

[9] W. Cazcarra and P. Zunino, J. Appl. Phys. **51**, 4206 (1980).

[10] S.T. Lee, P. Fellinger, and S. Chen, J. Appl. Phys. **63**, 1924 (1988).

[11] S.A. McQuaid, M.J. Binns, C.A. Londos, J.H. Tucker, and A.R. Brown, J. Appl. Phys. **77**, 1427 (1995).

[12] H. Takeno, Y. Hayamizu, and K. Miki, J. Appl. Phys. **84**, 3113 (1998).

[13] V.P. Markevich, L.F. Makarenko, and L.I. Murin, Phys. Status Solidi A **93**, K173 (1986).

[14] M. Claybourn and R.C. Newman, Appl. Phys. Lett. **51**, 2197 (1987).

[15] T. Hallberg and J.L. Lindström, J. Appl. Phys. **79**, 7570 (1996).

[16] T. Hallberg and J.L. Lindström, Mater. Sci. Eng. B **36**, 13 (1996).

[17] R. C. Newman, in *Early Stages of Oxygen Precipitation in Silicon* (Ref. 1), p. 19.

[18] L.I. Murin, T. Hallberg, V.P. Markevich, and J.L. Lindström, Phys. Rev. Lett. **80**, 93 (1998).

[19] T. Hallberg, J.L. Lindström, L.I. Murin, and V.P. Markevich, Mater. Sci. Forum **258-263**, 361 (1997).

[20] D. Åberg, B.G. Svensson, T. Hallberg, and J.L. Lindström, Phys. Rev. B **58**, 12 944 (1998).

[21] U. Gösele and T.Y. Tan, Appl. Phys. A: Solids Surf. **A28**, 79 (1982).

[22] L. I. Murin and V. P. Markevich, in *Early Stages of Oxygen Precipitation in Silicon* (Ref. 1), p. 329.

[23] M.P. Guse and R. Kleinhenz, J. Appl. Phys. **72**, 4615 (1992).

[24] Y.J. Lee, J. von Boehm, M. Pesola, and R.M. Nieminen, Phys. Rev. Lett. **86**, 3060 (2001); Y.J. Lee, J. von Boehm, and R.M. Nieminen, Appl. Phys. Lett. **79**, 1453 (2001).

[25] L.C. Snyder, J.W. Corbett, P. Deák, and R. Wu, Mater. Res. Soc. Symp. Proc. **104**, 179 (1988).

[26] C. P. Ewels, R. Jones, and S. Öberg, in *Early Stages of Oxygen Precipitation in Silicon* (Ref. 1), p. 141.

[27] M. Ramamoorthy and S. Pantelides, Phys. Rev. Lett. **76**, 267 (1996).

[28] M. Ramamoorthy and S.T. Pantelides, Solid State Commun. **106**, 243 (1998).

[29] J. Coutinho, R. Jones, P.R. Briddon, and S. Öberg, Phys. Rev. B **62**, 10 824 (2000).

[30] Y. J. Lee, J. von Boehm, and R. M. Nieminen (unpublished).

[31] P. Hohenberg and W. Kohn, Phys. Rev. **136**, B864 (1964).

[32] W. Kohn and L.J. Sham, Phys. Rev. **140**, A1133 (1965).

[33] S. Pöykkö, M.J. Puska, and R.M. Nieminen, Phys. Rev. B **57**, 12 174 (1998).

[34] R. M. Nieminen, in *Current Opinion in Solid State and Materials Science*, (Elsevier, New York 1999), Vol. 4, No. 6, p. 493.

[35] J. Perdew and A. Zunger, Phys. Rev. B **23**, 5048 (1981).

[36] D.M. Ceperley and B.J. Alder, Phys. Rev. Lett. **45**, 566 (1980).

[37] D.H. Hamann, Phys. Rev. B **40**, 2980 (1989).

[38] L. Kleinman and D.M. Bylander, Phys. Rev. Lett. **48**, 1425 (1982).

[39] D. Vanderbilt, Phys. Rev. B **41**, 7892 (1990).

[40] M. Pesola, J. von Boehm, and R.M. Nieminen, Phys. Rev. Lett. **82**, 4022 (1999).

[41] M. Pesola, J. von Boehm, T. Mattila, and R.M. Nieminen, Phys. Rev. B **60**, 11 449 (1999).

[42] M. Pesola, Y.J. Lee, J. von Boehm, M. Kaukonen, and R.M. Nieminen, Phys. Rev. Lett. **84**, 5343 (2000).

[43] R. M. Nieminen, M. Pesola, Y. J. Lee, and J. von Boehm, in *Computer Simulation Studies in Condensed Matter Physics*, edited by D. P. Landau, S. P. Lewis, and H. B. Schüttler (Springer-Verlag, Heidelberg, 2000), Vol. XIII.

[44] M. Kaukonen, P.K. Sitch, G. Jungnickel, R.M. Nieminen, S. Pöykkö, D. Porezag, and Th. Frauenheim, Phys. Rev. B **57**, 9965 (1998).

[45] M. Kaukonen, J. Peräjoki, R.M. Nieminen, G. Jungnickel, and Th. Frauenheim, Phys. Rev. B **61**, 980 (2000).

[46] M. Stavola, J.R. Patel, L.C. Kimerling, and P.E. Freeland, Appl. Phys. Lett. **42**, 73 (1983).

[47] G. D. Watkins, in *Early Stages of Oxygen Precipitation in Silicon* (Ref. 1), p. 1.

[48] J.M. Trombetta, G.D. Watkins, J. Hage, and P. Wagner, J. Appl. Phys. **81**, 1109 (1997).

[49] C. A. J. Ammerlaan, in *Properties of Crystalline Silicon*, edited by R. Hull (INSPEC, London, 1999), p. 663.

[50] J. L. Lindström and T. Hallberg, in *Early Stages of Oxygen Precipitation in Silicon* (Ref. 1), p. 41.

[51] T. Hallberg and J.L. Lindström, Appl. Phys. Lett. **68**, 3458 (1996).

[52] Ya.I. Latushko, L.F. Makarenko, V.P. Markevich, and L.I. Murin, Phys. Status Solidi A **93**, K181 (1986).

[53] A. Ourmazd, W. Schröter, and A. Bourret, J. Appl. Phys. **56**, 1670 (1984).

[54] G.H. Vineyard, J. Phys. Chem. Solids **3**, 121 (1957).

[55] V. Milman, M.C. Payne, V. Heine, R.J. Needs, J.S. Lin, and M.H. Lee, Phys. Rev. Lett. **70**, 2928 (1993).

[56] B. Sadigh, T.J. Lenosky, S.K. Theiss, M.-J. Caturla, T.D. de la Rubia, and M.A. Foad, Phys. Rev. Lett. **83**, 4341 (1999).